# Acoustic Radiation from Ends of IDT in Synchronous LSAW Resonators

V. Plessky[1,2], J. Koskela[1,2], B. A. Willemsen[2], P. J. Turner[2], R. B. Hammond[2], N. O. Fenzi[2],
[1]GVR Trade SA, Gorgier, Switzerland
[2]Resonant Inc., Santa Barbara, CA, USA 93117
Email: vplessky@resonant.com

***Abstract*—In order to minimize losses due to bulk-acoustic radiation, 'leaky' SAW resonators on rotated Y-cut $LiTaO_3$ typically employ synchronous design, with all the electrodes in the IDT and in the reflectors sharing the same periodicity and electrode shape. The change in the electric connection pattern between the IDT and the reflectors creates an electric discontinuity, which can serve as an additional source of bulk wave radiation. In this work, numerical FEM simulations are employed to characterize this additional loss mechanism.**

***Index Terms*—Surface Acoustic Waves; Finite Element Method; Numerical Modeling**

## I. Introduction

The leaky surface acoustic wave (LSAW) in rotated Y-cut $LiTaO_3$ and $LiNbO_3$ is a dominantly shear-horizontal wave, localized near the surface, and weakly coupled to the slow shear bulk-acoustic wave (BAW). Any surface perturbation can lead to radiation of bulk-acoustic waves from the device. To minimize such losses, LSAW resonators typical use synchronous design, with all electrodes in the IDT and in the reflectors having the same periodicity and shape. Moreover, the crystal cut and the thickness of the metallization are typically optimized to minimize the propagation loss [1] due to the BAW coupling. More recent multi-layered substrates [2]–[4] eliminate the acoustic radiation by converting the LSAW into a guided Lamb or shear horizontal wave, which propagates in a piezoelectric thin film, constrained from below by an acoustical mirror.

In this work, we employ hierarchical cascade-FEM method [5] to numerically simulate conventional $LiTaO_3$ resonators, TCSAW resonators on $LiNbO_3$ [6], and multilayered $LiTaO_3$ resonators [4]. Cascade-FEM efficiently utilizes the periodic block structure, which is typical to SAW devices. It enables rapid 2D simulation of finite SAW devices, including electric characterization, visualization of acoustic fields and power flow, and direct calculation of the Q-factor.

## II. Conventional $LiTaO_3$ Resonator

A synchronous resonator with $N_t$ = 121 electrodes in the IDT and $N_g$ = 40 electrodes in each reflector was simulated on conventional 42°YX-cut $LiTaO_3$ substrate. The parameters of the resonator were as follows: pitch 1 $\mu$m, metallization ratio 0.55, aluminum electrodes with thickness 160 nm, and aperture 40 $\mu$m. The Kovacs material constants were used for $LiTaO_3$ [7]. Material losses were modeled as viscous damping in the electrodes and the substrate.

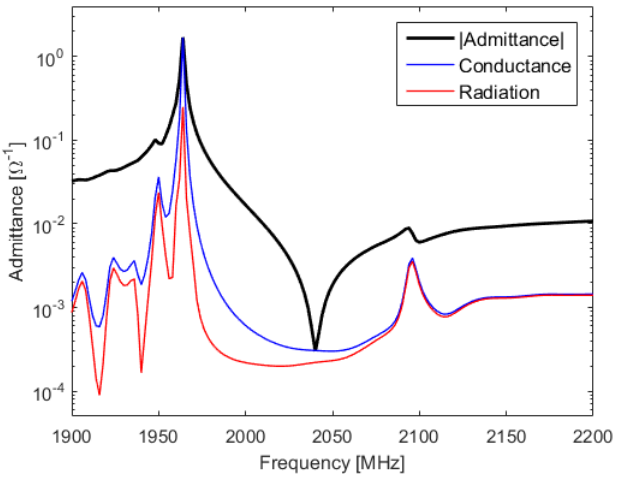


Fig. 1. Simulated frequency response of a LSAW resonator: admittance, conductance, and radiation contribution to the conductance.

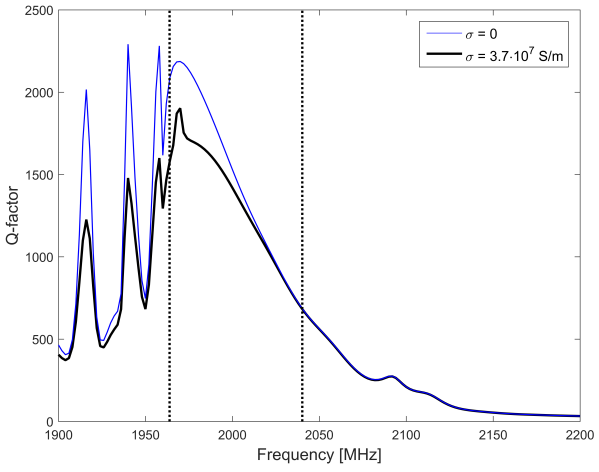


Fig. 2. Simulated Q-factor of a LSAW resonator, with and without resistivity. The dashed vertical lines indicate resonance and antiresonance.

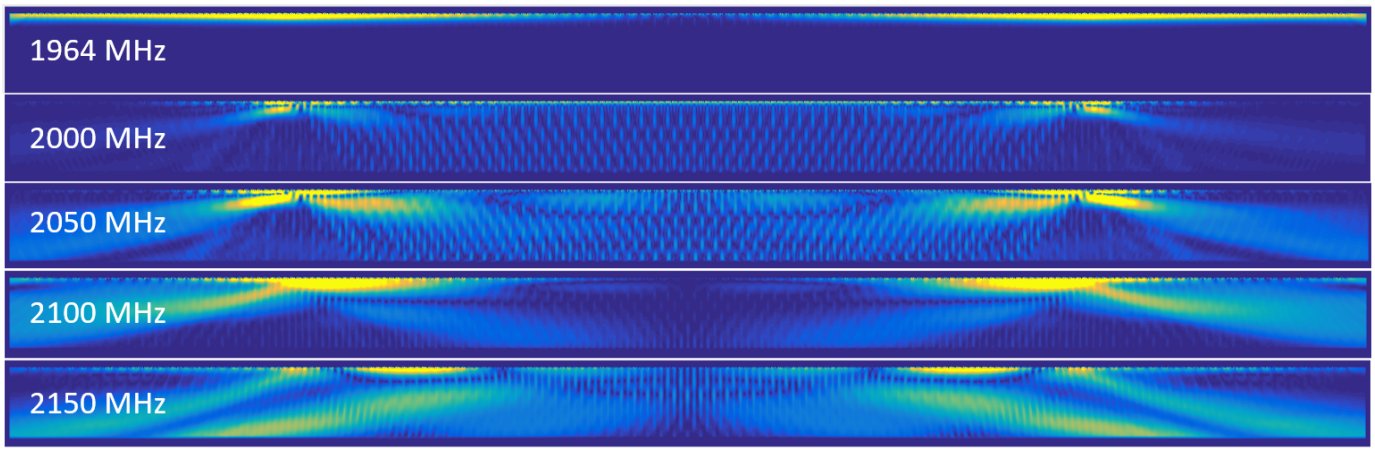


Fig. 3. Magnitude of acoustic power flow at different frequencies. A different color scale is used at different frequencies.

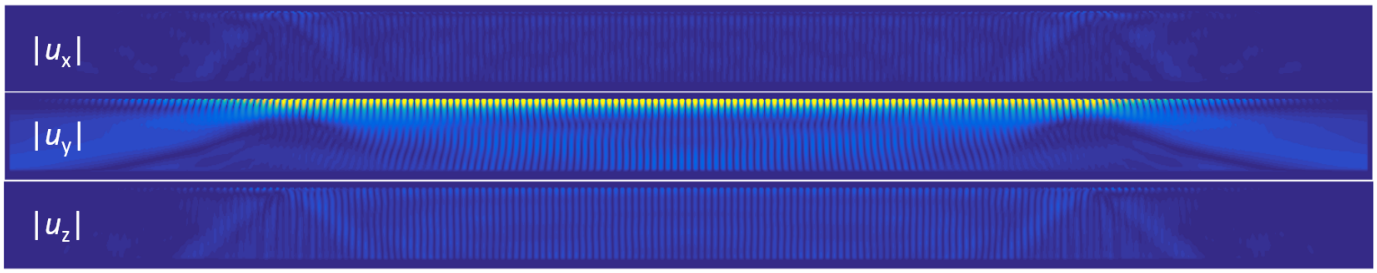


Fig. 4. Magnitude of mechanical displacement field visualized at 2050 MHz. All components are visualized using the same color scale.

The simulated frequency response is shown in Fig. 1. In addition to electric admittance, also the radiated power $P_{rad}$ was computed by integrating power flow across the mesh boundaries. The radiated power was converted in equivalent parallel conductance via $P_{\text{rad}} = G_{\text{rad}}|V|^2/2$, where $V$ denotes excitation voltage. The equivalent conductance is also shown in Fig. 1. Moreover, the piezoelectric energy stored in the device $\mathbf{E}$ was integrated over the simulation volume. It can be used to directly evaluate the quality factor $Q = 2\pi f\mathbf{E}/P_{tot}$, where $P_{tot} = \text{Re}(Y)|V|^2/2$. The obtained quality factor is shown in Fig. 2. For comparison, also a simulation with ideal conductivity is shown.

At the resonance frequency, acoustic radiation is insignificant and the Q-factor is limited by resistivity. However, radiation increases rapidly within the stopband and towards the synchronous threshold 2113 MHz. Radiation contributes substantially to losses at the antiresonance frequency. The power flow at various frequencies is visualized in Fig 3. Two different radiation mechanisms can be observed: fairly uniform radiation from the entire length of the IDT, and localized emissions from the ends of the IDT. The acoustic field at the antiresonance frequency is visualized in Fig. 4. The sagittal polarization and fairly deep propagation angle identify the distributed radiation as slow shear waves. In contrast, the radiation from the ends has dominantly shear-horizontally polarization, and it propagates in a shallow angle. These characteristics identify it as fast shear BAWs.

Because of the different nature of the radiation mechanisms, their relative significance depends on the length of the device. Fig. 5 shows the Q-factors for resonators with $N_t$= 61, 121, and 241 electrodes. The antiresonance Q-factor of the shortest resonator is only 60% of that of the longest resonator. This behaviour can be understood based on the electrode currents shown in Fig. 6. The real part of the electrode currents yields the conductance of the device–power losses. At the resonance, the currents are distributed across the whole device, and the current pattern is continuous across the reflector–transducer interface. In contrast, at the antiresonance the currents are concentrated around the ends of the IDT. A strong discontinuity appears: it covers the entire reflectors and about the first ten electrode pairs in the IDT. In particular, note the flip in the sign pattern between the first and second electrode in the reflector.

Moreover, the current pattern around the reflector-IDT boundary is almost identical in all resonators. Hence, the losses arising from this transition regime at the antiresonance are independent of the resonator length. In contrast, the stored energy and the cumulative propagation loss increase with resonator length.The longer the resonator, the less significant is the contribution from the edges. Here, taking the transition region to cover about the first ten electrode pairs of the IDT, the contributions from both edges for $N_t$ = 61, 121, and 241 is about 89%, 47%, and 24% of all losses, respectively. Note that this estimate contains not only radiation-related losses but

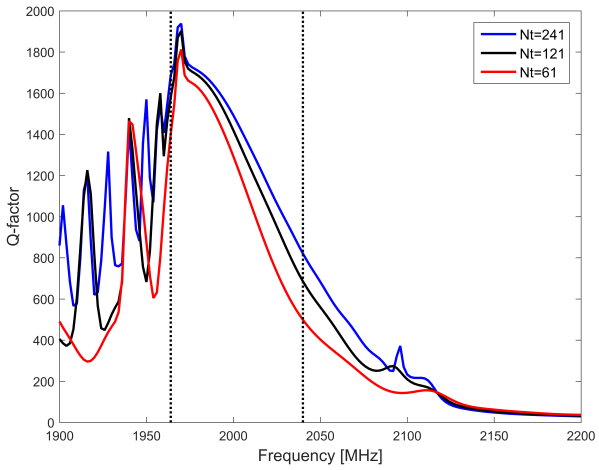


Fig. 5. Simulated Q-factors of LSAW resonators with different IDT length. The dashed vertical lines indicate resonance and antiresonance.

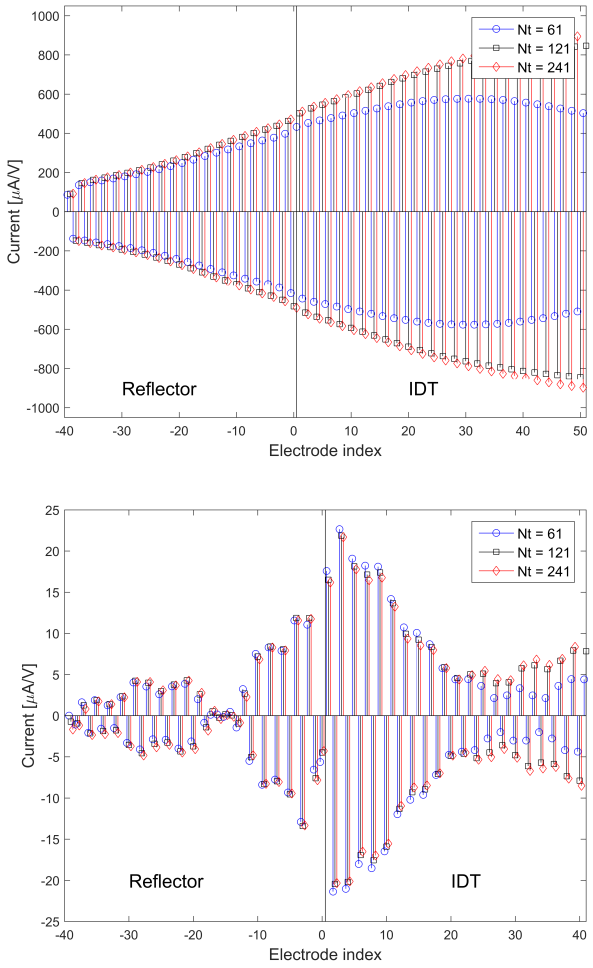


Fig. 6. Real part of electrode currents at $(top)$ resonance frequency and $(bottom)$ antiresonance frequency. Currents are shown for the first 80 electrodes; the sign of current is defined as the sign of net charge on the electrode. The pattern at the antiresonance is essentially the same regardless of device length.

also resistive losses and viscous damping.

## III. TCSAW Resonator

Typically, TCSAW devices employ 128°YX-cut $LiNbO_3$ substrate with copper electrodes and very thick $SiO_2$ overcoating [6]. The main mode is typically a classical Rayleigh-type wave. However, the layered structure supports various types of spurious modes, including shear horizontal SAW and plate modes. Hence, the TCSAW structure makes an interesting comparison point to LSAW resonators. A synchronous resonator with the following geometry was simulated: pitch 1 $\mu$m, metallization ratio 0.5, mostly Cu electrodes with thickness 170 nm, $SiO_2$ thickness 630 nm, acoustic aperture 49.2 $\mu$m, $N_t$ = 121 and $N_g$ = 40 electrodes. Kovacs material constants [7] were used for $LiNbO_3$.

The simulated electric response is shown in Fig. 6 and the Q-factor in Fig. 7. The stopband 1740 -1920 MHz is essentially clear of any acoustic radiation. The Q-factor remains high from the resonance to the antiresonance. The radiation loss below the resonance and in the range 1920-2030 MHz is SAWs escaping through the reflectors. Above 2050 MHz, BAW excitation contributes significantly to losses.

## IV. Plate-Mode $LiTaO_3$ Resonator

In the recently introduced incredible high performance SAW resonator (IHP) [3], [4], the radiation problem is solved by converting the LSAW into a guided shear-horizontal wave which propagates in a thin $LiTaO_3$ film. The film is confined from below by a reflecting $SiO_2$/AlN layer stack. According to our simulations, only a single $SiO_2$ layer between the $LiTaO_3$ thin film and the silicon substrate is sufficient to maximize the coupling and to eliminate BAW radiation in synchronous resonators. However, to control the spurious mode content, the layers must be very thin. Here we use pitch 1 $\mu$m and 8% Al electrodes; the $LiTaO_3$ layer is 1 $\mu$m thick, while the $SiO_2$ and AlN layers are 500 nm thick each.

The simulated frequency response for an IHP resonator is shown in Fig. 9, and the quality factor is shown in Fig. 10. The geometry of the device is same as in Fig. 1. The stopband is essentially free of all acoustic radiation, see Fig. 11. The Q-factor is determined by material losses and the waves escaping through the end reflectors. The simulated Q-factors are actually notably lower that the reported values, implying that the modeled viscous damping is too high; more accurate values should be determined experimentally. In the simulation, the most significant losses occur in the aluminum electrodes, and in the $LiTaO_3$ film.

## V. Conclusions

Losses in synchronous resonators have been analyzed with 2D FEM simulations. Cascade-FEM has proven a capable tool for visualizing and analysing loss mechanisms in complex layered SAW structures. In conventional LSAW resonators on $LiTaO_3$, the electric discontinuity between the IDT and the reflectors serves as a localized source of BAW radiation. This limits the achievable Q-factor; especially at the antiresonance, and in short resonators.

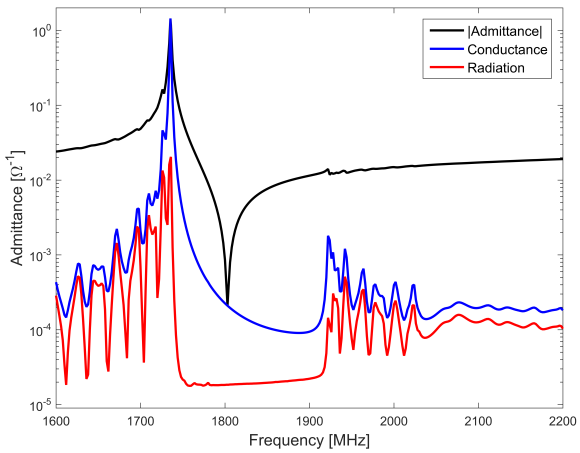


Fig. 7. Simulated frequency response of a TCSAW resonator: admittance, conductance, and radiation contribution to the conductance.

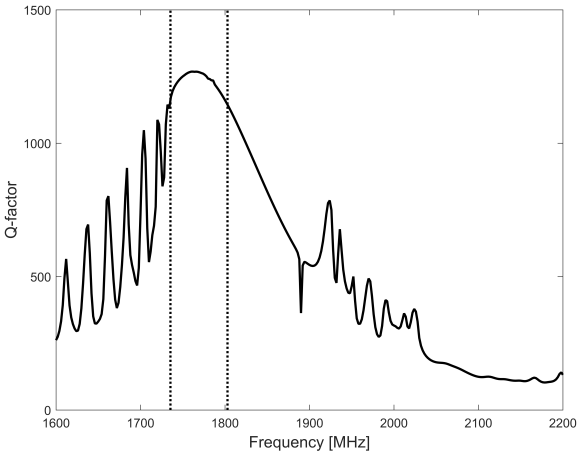


Fig. 8. Simulated Q-factor of a TCSAW resonator. The dashed vertical lines indicate resonance and antiresonance.

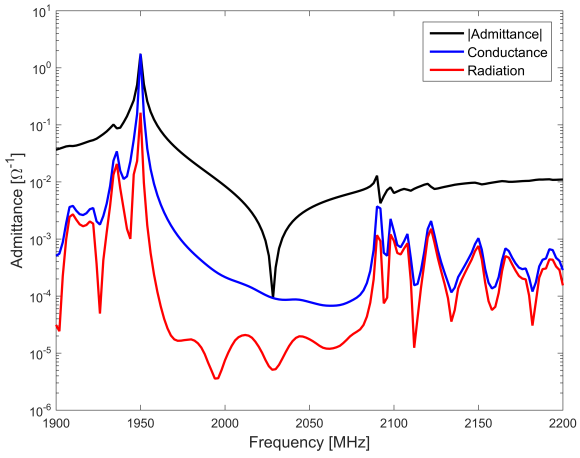


Fig. 9. Simulated frequency response of an IHP resonator: admittance, conductance, and radiation contribution to the conductance.

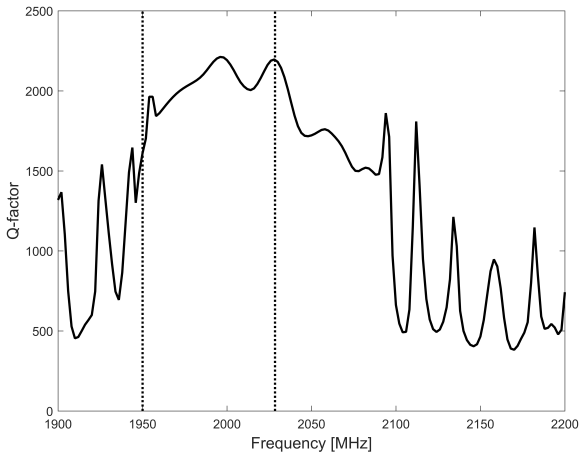


Fig. 10. Simulated Q-factor of an IHP resonator. The dashed vertical lines indicate resonance and antiresonance.

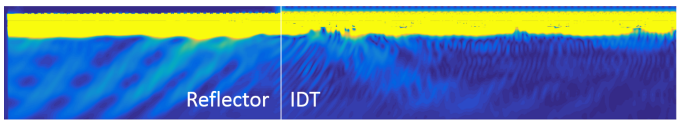


Fig. 11. Power flow in an IHP resonator at antiresonance, demonstrating weak residual bulk-wave radiation from the layer structure (intense power flow) into the silicon substrate (weak power flow). The resonator is symmetric; only the left half of the structure is shown.

## REFERENCES


[1] O. Kawachi, G. Endoh, M. Ueda, O. Ikata, K. Hashimoto, and M. Yamaguchi, *Optimum cut of $LiTaO_3$ for high performance leaky surafce acoustic wafe filters*, Proc. IEEE Ultrasonics Symp., 1996, pp. 71-76.

[2] M. Kadota and S. Tanaka, *HAL SAW Resonators Using $LiTaO_3$ Thin Plate on Quartz Substrate*, in Freq. Control Symposium 2017.

[3] M. Kadota and S. Tanaka, *Solidly Mounted Ladder Filter using Shear Horizontal Wave in $LiNbO_3$*, Proc. IEEE Freq. Cont. Symp., pp. 361-364, 2016.

[4] T. Takai, H. Iwamoto, Y. Takamine, H. Yamazaki, T. Fuyutsume, H. Kyoya, T. Nakao, H. Kando, M. Hiramoto, T. Toi, M. Koshino, N. Nakajima, *Incredible high performance SAW resonator on novel multi-layered substrate*, in 2016 IEEE Ultrasonics Symposium, 2016.

[5] J. Koskela, P. Maniadis, B.A.Willemsen, P.J.Turner, R.B.Hammond, N.O.Fenzi, and V. Plessky, *Hierarchical cascading in 2D FEM simulation of finite SAW devices with periodic block structure*, in 2016 IEEE Ultrasonics Symposium, 2016.

[6] B. Abbott, R. Aigner, A. Chen, K. Gamble, T. Kook, J. Kuypers, M. Solal, and K. Steiner, *High Q TCSAW, in Sixth International Symposium on Acoustic Wave Devices for Future Mobile Communication Systems*, Chiba University, Japan, 2015.

[7] G. Kovacs, M. Anhorn, H. E. Engan, G. Visintini, and C. C. W. Ruppel, *Improved material constants for $LiNbO_3$ and $LiTaO_3$*, Proc. 1990 IEEE Ultrasonics Symp., pp. 435-438, 1990.